Regional conductance map of Saurashtra and surrounding regions

P. B. V. Subba Rao*, A. K. Singh and C. K. Rao

Indian Institute of Geomagnetism, Panvel, Navi Mumbai 410 218, India

Magnetovariational fields recorded by an array of magnetometers in Saurashtra and the surrounding regions have been analysed to infer the electrical conductivity distribution of the region. Only night-time magnetovariational fields were used because of the prevailing uniform source field conditions. Induction arrows (showing the relationship between vertical and horizontal magnetic field variations) are pointing towards Saurashtra and Kutch offshore basins.

Thin-sheet modelling of the observed induction arrows suggest the presence of two prominent conductivity anomalies. The first elongated anomaly coincides with the horst and graben offshore structures of Saurashtra and Kutch. The second anomaly is over the Saurashtra depression and correlates well with the low-magnetization anomaly that extends in the NE–SW direction towards Cambay basin.

The possible cause for the above anomalies may be fluids originated by underplating mantle material related to hotspot activity and rift phase volcanism. Large-scale upwelling, partial melts or thermal remobilization of crustal and mantle material during the processes of rifting and hotspot activity may enhance crustal/upper mantle conductivity, which explains the accentuation of the induction arrows observed in Saurashtra region.

Keywords: Electrical conductivity, geomagnetic depth sounding, hotspot volcanism, rifting.

THE Saurashtra peninsula and the Cambay basin are two important geological regions in western India. The Saurashtra region occurs as a horst bounded by the Cambay rift basin (CRB) in the east, Narmada rift basin (NRB) in the south and Kutch rift basin (KRB) in the north[1]. Major geological and tectonic events of the Saurashtra region are confined to Mesozoic and Cenozoic eras and are associated with: (i) break-up of Africa from the Indian block containing Madagascar and Seychelles; (ii) later break-up of Madagascar from India due to Marion hotpot activity[2] and (iii) break-up of the Seychelles plateau from India[3] followed by eruption of Deccan volcanism related to interaction of Reunion hotspot activity[4,5]. Thus, the passive continental margin of western India has the imprint of two hotspots – Marion and Reunion, evolved through several stages of rifting–crustal thinning[6,7], magmatic underplating[8,9] and transient thermal effects[6].

*For correspondence. (e-mail: srao@iigs.iigm.res.in)

The western continental margin of India (WCMI) developed after break-up of west Gondwanaland splitting Madagascar and India. A series of rifts and graben formed parallel to the west coast. Major events that affected the basins on the western margin of India are: (i) rifting from Madagascar; (ii) Deccan/Reunion plume initiation with associated uplift (extension and subsidence), and (iii) drifting of the Indian plate towards north and resultant tectonic reactivation[10]. When the Indian plate collided with the Eurasian plate, its velocity decreased considerably and intraplate forces dormant till then started to play a leading role. The combined effect of these forces led to rifting and shearing along the west coast basins. It is widely believed that Deccan volcanism originated during Gondwanaland break-up (Seychelles–India separation) ca. 65 Ma (refs 11–13).

The three offshore sedimentary basins in northwestern India are Kutch, Saurashtra and Mumbai offshore basins (Figure 1 *b*). These offshore basins are characterized by a wide shelf with 7–8 km thick sedimentary cover[14]. Several longitudinal extensional faults in parallel sets have been responsible for the widening of the shelf and differentiating into several marginal basins. These rift basins and igneous intrusions close to the west coast of India and adjoining regions developed after the break-up of Gondwanaland during the Mesozoic period[1,3].

The Saurashtra peninsula is a horst structure (uplifted) that has witnessed various tectonic activities such as deviatorial forces causing inter-continental splitting, different phases of rifting, reactivation of the ancient fault zones and Deccan volcanism due to Reunion plume activity[1]. Major portion of the region is occupied by Deccan lava flows (Figure 1 *a*). The general stratigraphy of the peninsula consists of a Precambrian basement overlain by Mesozoic sediments followed by Deccan traps. A thin cover of Neogene and Quaternary sediments occurs at the top. A number of volcanic plugs in the west (Junagadh, Barda, Alech) and in the southeast (Chogat, Chamardi) have been reported in this region. These volcanic plugs are composed of tholeiites with several intrusions of acidic, alkaline and mafic/ultramafic plugs[15].

The Saurashtra depression is a ENE–WSW trending elongated feature in the offshore area, which is in lateral continuity of the Narmada–Tapti rift zone. Later subsidence of this depression occurred as India moved off the hotspot[16]. The Saurashtra depression is filled with ~ 8 km thick Tertiary, fine-grained, clastic sediments and is the main source rock for the Bombay Platform hydrocarbons[17,18].

Electromagnetic (EM) fields are widely used to study the geodynamic processes of the earth due to their ability to penetrate deep into the earth and resolve the electrical conductivity of complex geological structures[19,20]. As the western margin of India has been affected by the episodes of rifting and hotspot activity, magnetovariational study also known as geomagnetic depth sounding (GDS) was

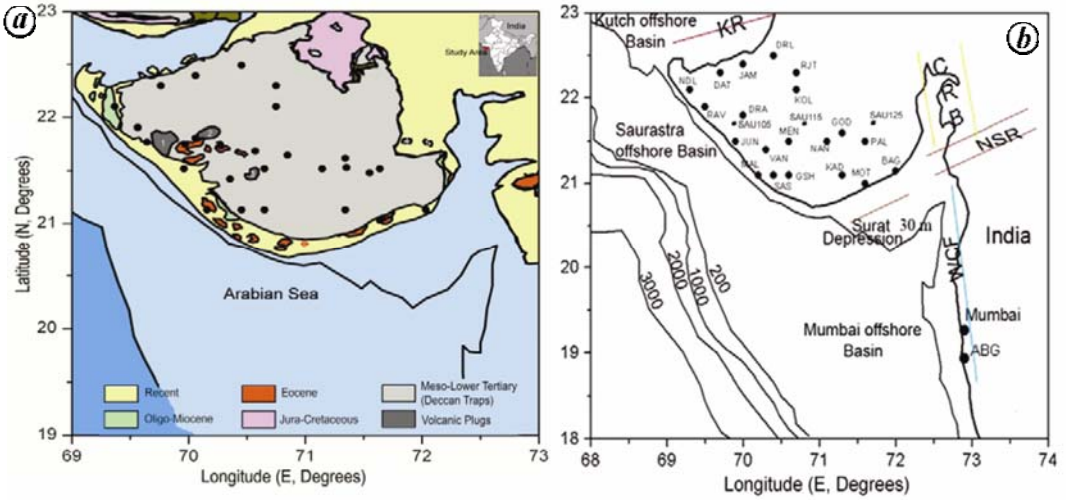

Figure 1. ***a***, Geological map of Saurashtra and the surrounding regions (after Merh[15]). Various fluxgate magnetometer stations installed in different phases are shown. Volcanic plugs are (1) Girnar, (2) Barda, (3) Alech, (4) Chogat and (5) Chamardi (after Rao and Tewari[27]). ***b***, Various tectonic features of the western margin of India (after Biswas[43]) are: WCF, west coast fault; NSR, Naramada–Son rift basin; CRB, Cambay rift basin; KR, Kutch rift basin. The three character stations codes are NDL, Ran; DAT, Vachie; JAM, Jamnagar; DRL, Drol; RAV, Raval; DRA, Drapa; KOL, Kolitana; RJT, Rajkot; JUN, Mahiyan; VAN, Vanthali; MEN, Mesvan; GOD, Godhada; PAL, Palitana; Mal, Maliya; SAS, Sassan; GSH, Godashyam; KAD, Kadur; MOT, Motakuntvada; BAG, Bagdhana.

carried out at 20 different stations to understand the lateral electrical conductivity distribution in the Saurashtra region.

GDS uses natural geomagnetic transient variations to image the earth's interior in terms of lateral electrical conductivity contrasts. Data are collected by an array of magnetometers that are operated simultaneously in the study area. In this study, we present the results obtained from the GDS experiment carried out in Saurashtra region.

Magson fluxgate magnetometers were deployed at 20 different sites (Figure 1 *b*) for recording magnetic field variations with a sampling interval of 10 s. In principle, magnetovariational fields observed at any recording site can be considered to be composed of normal and anomalous parts. If *Xn*, *Yn* and *Zn* and *Xa*, *Ya* and *Za* represent the components of the normal field and anomalous field respectively, then the magnetic field components at any site (*Xs*, *Ys* and *Zs*) can be separated into normal and anomalous parts[21] (e.g. $Xs = Xn + Xa$). Under the assumption of uniform source field for short-period fluctuations, when $Zn \approx 0$ and $Zs \approx Za$, the vertical field transfer functions (*Tzx* and *Tzy*) can be expressed by a linear combination of two horizontal components expressed as

$$Za = Tzx\ Xn + Tzy\ Yn.$$

Conventionally, the conductivity information contained in vertical transfer functions is extracted by presenting them as induction arrows. The magnitude of the induction (real/quadrature) arrow is given by

$$I = \text{Sqrt}\ (Tzx * Tzx + Tzy * Tzy),$$

and azimuth of the arrow by

$$\theta = \tan^{-1}\ (Tzy/Tzx).$$

As a matter of convenience, the direction of real arrows is reversed so that they point towards the region of high electrical conductivity. Hence, when these arrows are displayed for all the sites, they form a powerful tool to locate and define the trend of the involved conductivity structures[21–23]. We have selected local night-time variations to ensure that the source field conditions are satisfied. The vertical field transfer functions are estimated using 8–12 events (depending on data availability at each site). Using the above equation, the vertical field transfer functions were computed for the period range 8–128 min using robust technique[24]. This enables us to study the behaviour of induction arrows with increasing period.

Induction arrows (real and quadrature) corresponding to the periods 8, 16, 26, 43 and 57 min are shown in Figure 2. The observed induction pattern is partly controlled by bathymetric trend and local conductivity. For short periods, the real induction arrows with their NW orientation (in the NW part of the array) point at right angle to the Kutch offshore basin, whereas in the southern part of the array these arrows are pointing towards the offshore basins of Narmada and Saurashtra. With increasing period (19 min onward) induction arrows rotate anticlockwise in the NW part of the array and rotate in clockwise direction in the southern part of the array to point towards the Saurashtra depression. This anomalous

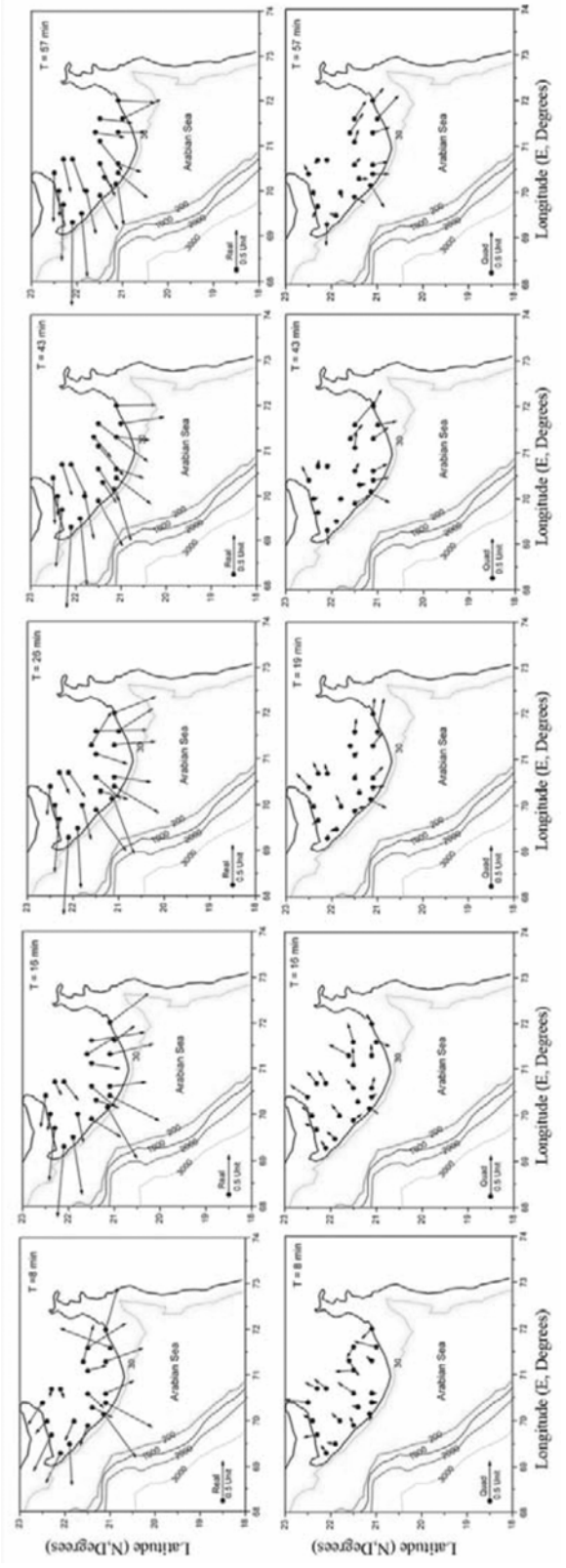

Figure 2. Observed induction arrows for 8, 16, 26, 43 and 57 min periodicities for the Saurashtra array. These induction arrows are pointing towards the Gulf of Kutch, Saurashtra offshore region and Gulf of Cambay having high conducting sedimentary basins. At higher periods, these induction arrows are rotating from NE to SW direction indicating the presence of anomalous conducting zone beneath the Saurashtra depression.

directional behaviour of the induction arrows suggests a large-scale electrical conductivity anomaly in the offshore region immediately SW of the Saurashtra region and is mapped using thin-sheet modelling by taking magnetotelluric studies into consideration.

Magnetotelluric sounding provides a way to determine the electrical conductivity image of the subsurface by simultaneous measurement of natural electric and magnetic field variations. For a general 3D variation, horizontal electric (*Ex*, *Ey*) and magnetic (*Hx*, *Hy*) fields at a given frequency are related through[25]

$$\begin{pmatrix} Ex \\ Ey \end{pmatrix} = Z \begin{pmatrix} Hx \\ Hy \end{pmatrix},$$

where Z (impedance tensor) is a complex tensor in frequency domain

$$Z = \begin{pmatrix} Zxx & Zxy \\ Zyx & Zyy \end{pmatrix}.$$

Apparent resistivity and phases are computed from the impedance tensor (Z) as

$$\rho_{ij} = \frac{1}{\omega\mu} | Z_{ij} | **2,$$

$$\phi_{ij} = \arctan(\mathrm{Im}(Z_{ij}) / \mathrm{Re}(Z_{ij})),$$

where $i = 1, 2$ and $j = 1, 2$.

Figure 3 shows apparent resistivity (ρ_{xy} and ρ_{yx}) and phases (ϕ_{xy} and ϕ_{yx}) from 0.001 to 1000 s, and 1D resistvity depth section (using Occams inversion)[26] for the three representative sites SAU-105, SAU-115 and SAU-125 located in the western, central and eastern parts of the Saurashtra region. The one-dimensional model suggests that the topmost resistivity layer of 100 Ωm occurring at high frequency corresponds to Deccan volcanics having a thickness of about 1 km. The second layer, with the resistivity range 50 Ωm occurring at frequency ranges lower than that of the volcanics corresponds to Mesozoic sediments. The layer of high resistivity (5000 Ωm) at lower frequency corresponds to the upper crust (5–20 km). This may represent volcanic/granite crust. According to DSS studies[27], SAU-105 and SAU-115 are located over the volcanic crust and SAU-125 is located over the granite upper crust. Similarly, a high resistive body has also been inferred in other regions of the Deccan volcanic province, viz. at the epicentral zone of Valsad, Gujarat[28] and in the Kurdwadi–Koyna region[29–32]. The lower crust is moderately resistive (200–500 Ωm) and thickness of the lithosphere varies from 100 to 120 km as shown in Figure 3.

To obtain the electrical conductivity distribution that simulates the observed induction response, a 3D

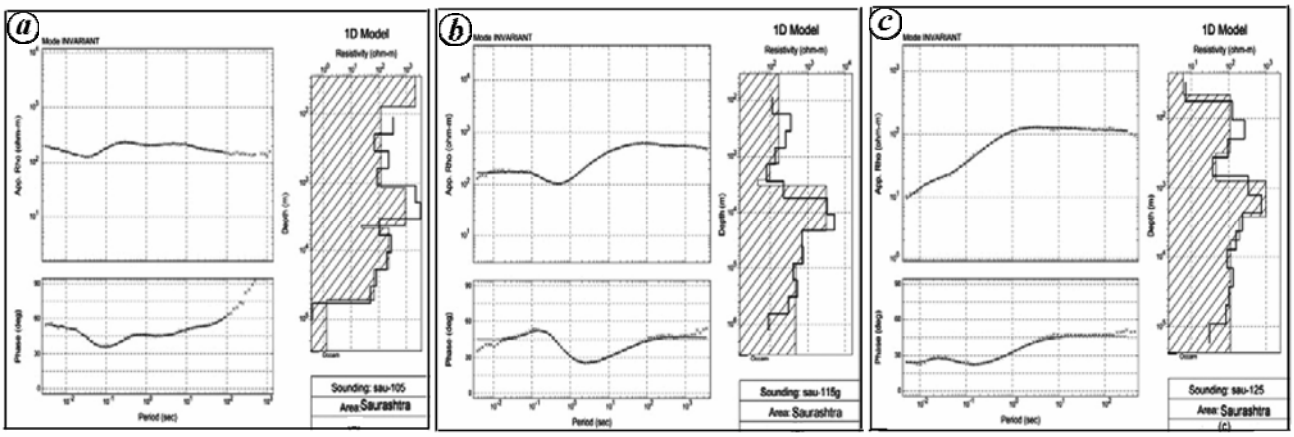

Figure 3 *a*–*c*. One-dimensional model obtained for the MT sites SAU-105, SAU-115 and SAU-125 using Occams inversion. This model indicates that the top layer is Deccan volcanic having a thickness of about 1 km, the second layer consists of Mesozoic sediments extending to a depth of about 5 km and is underlain by a high resistive underplating material.

thin-sheet forward modelling approach has been adopted. This thin-sheet formulation considers that the conductivity anomalies are confined to a single layer on the surface of the earth. In such cases, the mathematical model comprises an infinitesimally thin sheet of varying surface conductance underlain by a layered half space.

In modelling the regional data equivalent thickness is usually assigned, such that the conductance may be thought of as the conductivity integrated vertically through the thickness of the sheet. The limit on the thickness of the sheet is provided by the conductivity of the material constituting the sheet as well as by the linked electrical substratum, so that, at the periods of study the horizontal field remains constant over the thickness of the sheet[33,34]. This implies that the thickness of the sheet should be small compared to the skin depth of the diffusing EM wave in the layer immediately beneath the sheet at the considered period. Another condition is that the sheet thickness should be very small in relation to the skin depth in any material included in the sheet. In the numerical grid, node spacing should not be greater than one-third of the skin depth of the layer underlying the thin sheet. In the present study, the thin sheet was assigned a thickness of 5 km that allows incorporating bathymetry (depth of sea-water column) of the study area. This thin sheet layer was considered to overlie a three-layered structure: the top layer having a thickness of about 15 km and resistivity of about 1000 Ωm, the middle layer 90 km thick having a resistivity of about 500 Ωm that overlies a half space having resistivity 50 Ωm. The choice of the background layered structure was based on the 1D model as discussed earlier. Formulations approximating 3D structures in thin sheet approximation for regional studies have been developed earlier[35,36]. We used the program of Vasseur and Weidelt[35] for explaining the observed induction response of the Saurashtra region. Coast effect was estimated using thin sheet approximation to represent lateral variations arising from continental crust and sea water of variable depths. The conductance map was prepared by incorporating additional subsurface structures (using published geophysical inputs) to explain the observed induction pattern in the Saurashtra region.

For the purpose of numerical computation, an area between 18°–23°N and 68°–74°E was chosen and divided into 50 × 60 grid with a grid interval 11 km, i.e. one order less than the skin depth of the underlying layer beneath the thin sheet. The computations have been carried out for a period of 26 min, where the observed response is best observed. For calculating the coast effect, the thickness of the water column has been adopted from the bathymetry maps (Figure 4 *a*) published by the Naval Hydrographic Office[37]. The conductivity of sea water was taken as 0.33 Ωm (ref. 38). The above thin sheet was considered to be underlain by a geoelectrical structure as discussed earlier. Since a region of normal structure surrounds the anomalous zone, the artifacts due to the boundary are minimized by extending the grid to sufficiently large distances away from the observational domain[39]. In the present case the skin depth of the underlying layer by 26 min period is about 624 km and is much larger than the assumed thickness (5 km) of the anomalous surface layer. Similarly, the skin depth of the sea water is approximately 12 km, again about four times larger than the maximum depth of the sea water. The grid spacing is 11 km and satisfies the condition that it should be less than one-third of the skin depth of the underlying layer. Thus, the thin sheet satisfies all the conditions described[33].

For estimating the coast effect (i.e. arising due to land and sea water of variable depths) the numerical computations have been carried out for ten periods in the range 8–128 min. Figure 4 *b* shows the calculated real induction arrow pattern at 26 min. As seen in the figure, the calculated coast effect is significantly small as the shelf width

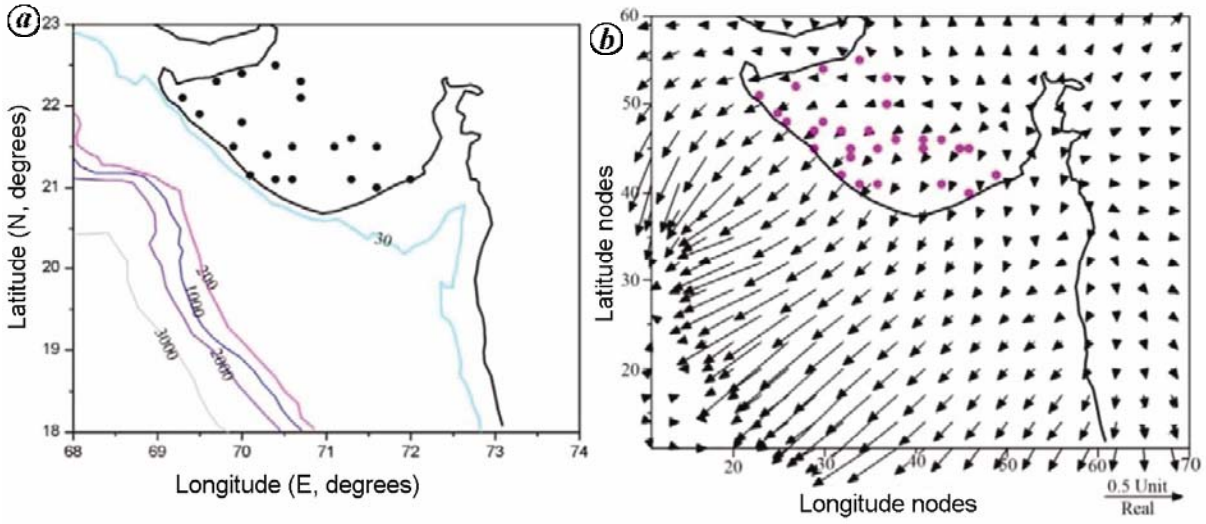

Figure 4. ***a***, Bathymetry map of Saurashtra and the surrounding regions. Depth of the sea water column is given in metres. ***b***, Real induction arrows for period = 26 min corresponding to the thin-sheet model depicting lateral variations due to sea water of variable depth. Arrows are shown for alternative grid points.

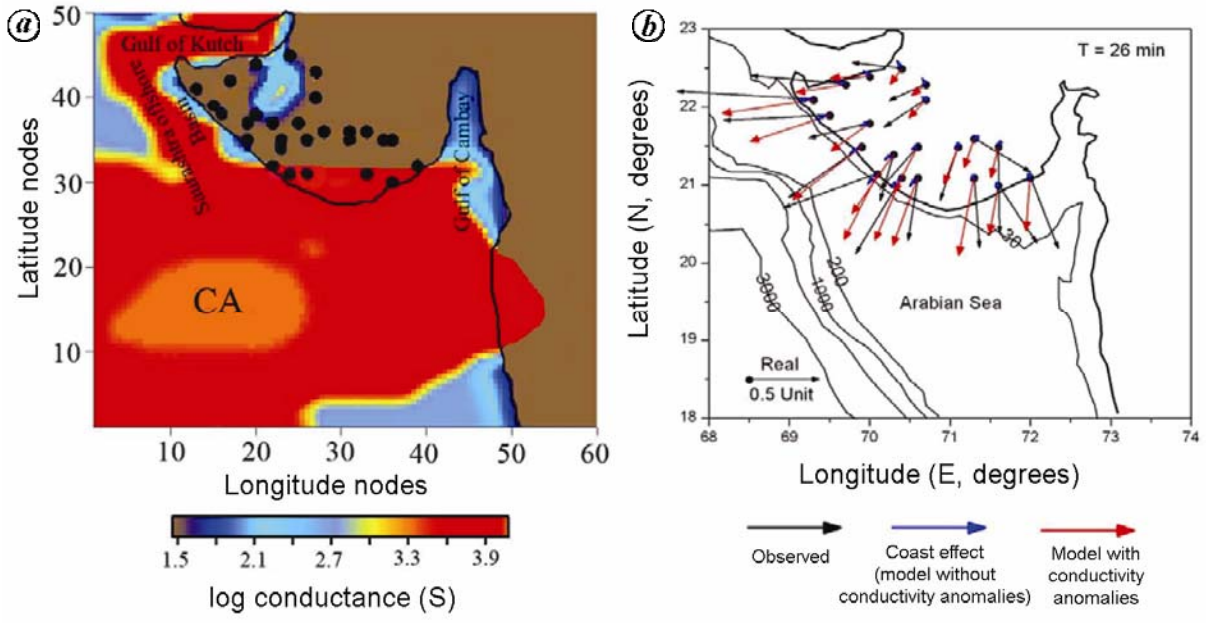

Figure 5. ***a***, Thin-sheet conductance map of Saurashtra and the surrounding regions. Different conductivity anomalies have been observed over the Gulf of Kutch, Saurashtra offshore basin and Gulf of Cambay. Most prominent anomaly (CA) is associated with the Saurashtra depression. ***b***, Comparison between the observed and calculated real induction arrows is shown for the 26 min period.

in this region is more than 250 km and the observed induction is dominantly controlled by offshore structures.

Taking the coast effect into account, the observed induction arrows have been explained in terms of high-conductivity anomaly (~ 15,000 S) running parallel to the coast of Saurashtra and the Gulf of Kutch. Towards the southern part of the array, high conductivity anomaly is observed over the Cambay basin and Saurashtra depression. Initial conductance values have been assigned to sedimentary basins based on 1D resistivity models obtained in Saurashtra region. The resistivity of sediments varies from 10 to 50 Ωm. Later, conductance cells in the offshore region have been changed in a trial and error procedure following the trend of low magnetization anomaly[40] and high thermal anomaly[41]. Figure 5 *a* shows the distribution of depth-integrated conductance values of about 4000–15,000 S, that best produces the induction response close to the observed induction pattern. The

calculated induction response obtained without incorporating the Saurashtra depression anomaly does not represent the observed induction arrows. However, inclusion of the Saurashtra depression anomaly brings a close semblance between the observed and calculated arrows, both in magnitude and direction. The fit is reasonably good near the southwestern part where the strongest anomaly pattern is observed. A comparison between observed and calculated induction arrows is shown in Figure 5 *b*.

The high conductivity anomaly over Saurashtra depression could be related to high conducting sediments and hydrous fluids released during various tectonic activities, which explains the accentuation of the observed induction arrows in the Saurashtra region. Similar regional-scale conductivity anomaly centred immediately SW of the southern tip of India due to the Marion hotspot activity has been mapped by Arora and Subba Rao[42].

The integrated modelling of the EM response functions from Saurashtra region has brought out high conductivity anomalies over the Saurashtra depression and offshore basins. The possible causes for these anomalies could be fluids originated by underplating mantle material related to rift phase volcanism and hotspot activity. The depth extent of the conductivity anomaly associated with the Saurashtra region remains elusive. It may be noted that the Saurashtra depression anomaly has been mapped from inland measurements only. New seafloor EM measurements around the Saurashtra offshore region will fulfil the need to map the electrical conductivity structures in more detail.

1. Biswas, S. K., Regional tectonic framework, structure and evolution of the western marginal basins of India. *Tectonophysics*, 1987, **135**, 307–327.
2. Storey, M., Mahoney, J. J., Saunders, A. D., Duncan, R. A., Kelley, S. P. and Coffin, M. F., Timing of hot spot related volcanism and the breakup of Madagascar from India. *Science*, 1995, **267**, 852–855.
3. Besse, J. and Courtillot, V., Paleographic maps of the continents bordering the Indian Ocean since the early Jurassic. *J Geophys. Res.*, 1988, **93**, 11791–11808.
4. White, R. S. and Mckenzie, D. P., Magmatism at rift zones: the generation of volcanic continental margins and flood basalts. *J. Geophys. Res.*, 1989, **94**, 7685–7729.
5. Naini, B. R. and Talwani, M., Structural framework and the evolutionary history of the continental margin of western India. *AAPG Mem.*, 1983, **34**, 167–191.
6. Biswas, S. K., Tectonic framework and evolution of graben basins of India. In *Rifted Basins and Aulacogens* (eds Casshyap, S. M. *et al.*), Gyanodaya Prakashan, Nainital, 1993, pp. 18–32.
7. McKenzie, D. P., Some remarks on the development of sedimentary basins. *Earth Planet. Sci. Lett.*, 1978, **40**, 25–32.
8. Cox, K. G., A model for flood basalt volcanism. *J. Petrol.*, 1980, **21**, 629–650.
9. Devey, C. W. and Lightfoot, P. C., Volcanology and tectonic control of stratigraphy and structure in the western Deccan Traps. *Bull. Volcanol.*, 1986, **48**, 195–207.
10. Gombos Jr, A. M., Powell, W. G. and Norton, I. O., The tectonic evolution of western India and its impact on hydrocarbon occurrences: an overview. *Sediment. Geol.*, 1995, **96**, 119–129.
11. Courtillot, V., Besse, J., Vandamma, D., Montingy, R., Jaeger, J. J. and Coppetta, H., Deccan flood basalts at the Cretateous/Tertiary boundary? *Earth Planet Sci. Letts.*, 1986, **80**, 361–374.
12. Venkateasan, T. R., Pande, K. and Gopalan, K., Did Deccan volcanism predate the K/T transition? *Earth Planet Sci. Lett.*, 1993, **119**, 181–189.
13. Collier, J. S., Sansom, V., Ishizuka, O., Taylor, R. N., Minshull, T. A. and Whitmarsh, R. B., Age of Seychelles–India break-up. *Earth Planet Sci. Lett*., 2008, **272**, 264–277.
14. Singh, K., Radhakrishna, M. and Pant, A. P., Geophysical structure of western offshore basins of India and its Implications to the evolution of the Western Ghats. *J. Geol. Soc. India*, 2007, **70**, 445–459.
15. Merh, S. S., *Geology of Gujarat*, Geological Society of India, Bangalore, 1995, pp. 1–222.
16. Bhattacharya, G. C. and Subrahmanyam, V., Extension of the Narmada–Son lineament on the continental margin off Saurashtra, western India as obtained from magnetic measurements. *Mar. Geophys. Res.*, 1986, **8**, 329–344.
17. Biswas, S. K. and Singh, N. K., Western continental margin of India and hydrocarbon potential of deep-sea basins. In 7th Offshore South East Asia Conference, Singapore, 1988, pp. 170–181.
18. Banerjee, V., Mittal, A. K., Gupta, A. K., Balyan, A. K. and Chaudhary, D. R., On the origin of hydrocarbons reservoired in Bombay High: stable isotopic studies of natural gases. *J. Southeast Asian Earth Sci.*, 1991, **5**, 339–343.
19. Gough, D. I., Magnetometer array studies, earth structure and tectonic processes. *Rev. Geophys.*, 1989, **27**, 141–157.
20. Arora, B. R., Seismotectonics of the frontal Himalaya through the electrical conductivity imaging. In *Seismotectonics in Convergent Plate Boundary* (eds Fujinawa, Y. and Yoshida, A.), Terra Scientific Publishing Company (TERRA PUB), Tokyo, 2002, pp. 261–272.
21. Schmucker, U., Anomalies of geomagnetic variations in the southwestern United States. *Bull. Scripps Inst. Oceanogr*., 1970, **13**, 1–165.
22. Beamish, D., The mapping of induced currents around the Kenya rift: comparison techniques. *Geophys. J. R. Astron. Soc*., 1977, **50**, 311–322.
23. Arora, B. R., Rigoti, A., Vitorello, I., Padhila, A. L., Trivedi, N. B. and Chamalaun, F. H., Electrical imaging of the intracratonic Parnaiba basin, North–Northeast Brazil. *J. Geomagn. Geoelectr.*, 1997, **49**, 1631–1648.
24. Egbert, G. D. and Booker, J. R., Imaging crustal structure in southwestern Washington with small magnetometer arrays. *J. Geophys. Res.*, 1993, **98**, 15967–15985.
25. Vozoff, K., The magnetotelluric method in the exploration of sedimentary basins. *Geophysics*, 1972, **37**, 98–141.
26. Constable, S., Parker, R. L. and Constable, C., Occam's inversion: a practical algorithm for generating smooth models from EM sounding data. *Geophysics*, 1987, **52**, 289–300.
27. Rao, G. S. P. and Tewari, H. C., The seismic structure of the Saurashtra crust in NW India and its relationship to Reunion hotspot. *Geophys. J. Int*., 2005, **160**, 318–330.
28. Arora, B. R. and Reddy, C. D., Magnetovariational study over a seismically active area in the Deccan trap province of western India. *Phys. Earth Planet. Inter.*, 1991, **66**, 118–131.
29. Gokarn, S. G., Rao, C. K., Gupta, G., Singh, B. P. and Yamashita, M., Deep crustal structure in central India using magnetotelluric studies. *Geophys. J. Int.*, 2001, **144**, 685–694.
30. Sarma, S. V. S., Patro, B. P. K., Harinarayana, T., Veeraswamy, K., Sastry, R. S. and Sarma, M. V. C., A magnetotelluric (MT) study across the Koyna seismic zone, western India: evidence for block structure. *Phys. Earth Planet. Inter*., 2004, **142**, 23–36.
31. Patro, B. P. K. and Sarma, S. V. S., Trap thickness and the subtrappean structures related to mode of eruption in the Deccan Plateau of India: results from magnetotellurics. *Earth Planet Space*, 2007, **59**, 75–81.

32. Harinarayana, T., Patro, B. P. K., Veeraswamy, K., Manoj, C., Naganjaneyulu, K., Murthy, D. N. and Virupakshi, G., Regional geoelectric structure beneath Deccan Volcanic Province of the Indian subcontinent using magnetotellurics. *Tectonophysics*, 2007, **445**, 66–80.
33. Weaver, J. T., Regional induction in Scotland; and example of three-dimensional numerical modeling using the thin sheet approximation. *Phys. Earth Planet. Inter.*, 1982, **28**, 161–180.
34. Agarwal, A. K. and Weaver, J. T., Regional electromagnetic induction around the Indian peninsula and Sri Lanka; a three-dimensional numerical model study using the thin sheet approximation. *Phys. Earth Planet. Int.*, 1989, **54**, 320–331.
35. Vasseur, G. and Weidelt, P., Bimodel electromagnetic induction in nonuniform thin sheets with an application to the northern Pyrenean induction anomaly. *Geophys. J. R. Astron. Soc.*, 1977, **51**, 669–690.
36. Dawson, T. W. and Weaver, J. T., Three-dimensional induction in a non-uniform thin sheet at the surface of a uniformly conducting earth. *Geophys. J. R. Astron. Soc.*, 1979, **59**, 445–462.
37. NHO, Bathymetry maps published by the Naval Hydrographic Office, Dehradun, India, 1977.
38. Wannamaker, P. E. *et al.*, Fluid and deformation regime of an advancing subduction system at Marlborough, New Zealand. *Nature*, 2009, **460**, 733–736.
39. Mareschal, M., Vasseur, G., Srivastava, B. J. and Singh, R. N., Induction models of southern India and effect of offshore geology, *Phys. Earth Planet. Inter.*, 1987, **45**, 137–148.
40. Singh, B. P., Rajaram, M. and Bapat, V. J., Definition of the continent–ocean boundary of India and the surrounding oceanic regions from Magsat data. *Tectonophysics*, 1991, **192**, 145–151.
41. Rao, Y. H., Subrahmanyam, C., Sharma, R., Rastogi, A. A. and Deka, B., Estimates of geothermal gradients and heat flow from BSRs along the Western Continental Margin of India. *Geophys. Res. Lett.*, 2001, **28**, 355–358.
42. Arora, B. R. and Subba Rao, P. B. V., Integrated modeling of EM response functions from peninsular India and Bay of Bengal. *Earth Planets Space*, 2002, **54**, 637–654.
43. Biswas, S. K., A review of structure and tectonics of Kutch basin, western India, with special reference to earthquakes. *Curr. Sci.*, 2005, **88**, 1592–1600.

ACKNOWLEDGEMENTS. We are grateful to the Director, Indian Institute of Geomagnetism, Navi Mumbai for keen interest and financial support to carry out this work. We also thank Prof. B. R. Arora for fruitful discussions.

Received 20 September 2011; revised accepted 11 June 2012

Evidence of functional specialization and pollination syndrome in *Amomum subulatum* Roxb. (Zingiberaceae)

Kundan Kishore[1,*], H. Kalita[2], D. Rinchen[2] and Boniface Lepcha[2]

[1]Directorate of Research on Women in Agriculture, Baramunda, Bhubaneswar 751 003, India
[2]ICAR Research Complex for NEH Region, Sikkim Centre, Tadong, Gangtok 737 102, India

Here we study functional specialization in *Amomum subulatum* in recruiting specific pollinators and in exhibiting pollination syndrome. Among diverse assemblages of animals, only native bumble-bees (*Bombus braviceps* Smith and *Bombus haemorrhoidalis* Smith) acted as effective pollinators in terms of visitation frequency, pollination efficiency, pollination potential index, pollen delivery and fruit set, whereas *Udaspes folus* and *Macroglossum* sp. acted as nectar robbers and *Apis cerena* and *Episyrphus balteatus* were pollen-resource wasters. Native bumble-bee were the sole functional group that increased the plant's fitness by being the 'most effective pollinators'. Foraging behaviour is the most crucial factor to bring about pollination in *A. subulatum*. Medium tongue length and proficient nectar-foraging behaviour make bumble-bees the most effective pollen vectors. Low secretion rate of nectar during morning hours could be the strategy of plants to bring about pollination effectively by instigating medium-tongued nectar foragers to move deep inside the labellum and the anther–stigma column. *A. subulatum* may be categorized as an obligate specialist as it recruits only the bumble-bee as the most effective pollinator, thereby giving evidence of pollination syndrome.

Keywords: *Amomum subulatum*, functional specialization, nectar robber, pollination syndrome.

KÖLREUTER[1] and Darwin[2] had elaborated the views of plant–pollinator interaction, and gave an indication of specialization and recruitment of specific groups of pollinators by plants. Plant guilds with similar suites of floral traits might have evolved in order to attract and utilize specific functional groups of pollinators[3–5]. The markedly similar plants within these guilds are often only distantly related, suggesting independent and often convergent evolution of floral traits to match the traits of their common pollinators – one of the most visual testimonies to natural selection[6–8]. However, different pollinators promote selection for diverse floral forms giving rise to 'pollination syndrome', which is defined as a suite of floral traits, including rewards, associated with the attraction and utilization of specific 'functional groups' of pollina-

*For correspondence. (e-mail: kkhort2003@yahoo.com)